Available online at www.sciencedirect.com

ScienceDirect

Ceramics International 41 (2015) 12073–12080

CERAMICS INTERNATIONAL

www.elsevier.com/locate/ceramint

Visible-light photocatalysis with bismuth titanate ($Bi_{12}TiO_{20}$) particles synthesized by the oxidant peroxide method (OPM)

André E. Nogueira[a,*], Elson Longo[b], Edson R. Leite[a], Emerson R. Camargo[a]

[a]LIEC-Laboratório Interdisciplinar de Eletroquímica e Cerâmica, Departamento de Química, UFSCar-Universidade Federal de São Carlos, Rod.Washington Luis km 235, CP 676 São Carlos, SP 13565-905, Brazil

[b]Instituto de Química de Araraquara, UNESP-Universidade Estadual Paulista, Rua Francisco Degni, CP 355 Araraquara, SP 14801-907, Brazil

Received 1 May 2015; received in revised form 2 June 2015; accepted 4 June 2015
Available online 19 June 2015

Abstract

In this paper, we have successfully synthesized high quality single crystalline bismuth titanate with sillenite ($Bi_{12}TiO_{20}$) phase by the oxidant peroxide method (OPM). The structures of precipitate and calcined materials were characterized by X-ray diffraction (XRD), UV–vis diffuse reflectance spectra (DRS), X-ray photoluminescence (PL) spectroscopy, thermogravimetry analysis (TG), differential scanning calorimetry (DSC) Fourier transform infrared spectroscopy (FTIR), transmission electron microscope (TEM), scanning electron microscopy (SEM) and nitrogen adsorption/desorption. The XRD analysis showed that the calcination temperature of 500 °C and time of 1 h was found to be sufficient to produce $Bi_{12}TiO_{20}$ powder and the DRS confirmed that the photoresponse of the prepared bismuth titanate extended to the visible light region at about 465 nm representing a possible photoactivity under solar irradiation. The photocatalytic activities were verified through the photocatalytic degradation of rhodamine b (RhB) as a model compound under visible light irradiation. It was found that the material calcined at 400 °C exhibits good photocatalytic activity compared to commercial TiO_2, the kinetic rate constant over 400 °C is 0.006 min^{-1}, which is 9.4 times higher than commercial TiO_2. The higher photocatalytic activity of this material is mainly attributed to an increase in the extension of its optical absorption spectrum, as compared to TiO_2.
© 2015 Elsevier Ltd and Techna Group S.r.l. All rights reserved.

Keywords: A. Powders: chemical preparation; C. Optical properties; $Bi_{12}TiO_{20}$; Photocatalysis

1. Introduction

Photocatalytic processes based on semiconductors functioning as photocatalysts have been widely used as promising techniques in ecosystem protection due to their high efficiency for degradation of various organic pollutants under mild conditions. Some materials have been found and applied to the photocatalytic degradation of organic contaminants in both gas and liquid phases under visible-light irradiation [1–4].

A good photocatalyst should absorb photons whose energy is equal to or more than the band gap, thereby transferring an electron from the valence band into the conduction band and subsequently generating an electron–hole pair. These electrons and holes react with oxygen and water, producing superoxide anion radicals ($O_2^{\bullet -}$) and hydroxyl radicals ($HO^{\bullet}$) which act as stronger reducing and oxidizing species, respectively, thereby resulting in degradation of several organic compounds [3].

In order to achieve efficient visible light utilization, the discovery of active visible light-driven photocatalysts has attracted much attention. Recently, numerous oxides such as Ag_2ZrO_3, Bi_2O_3/g-C_3N_4, Bi_2WO_6, and $Bi_{12}TiO_{20}$ have been reported to show high activities [5–8].

$Bi_{12}TiO_{20}$ belongs to a family of sillenite compounds. This sillenite is formed by Bi–O polyhedra, where Bi ions are coordinated with five oxygen ions that form an octahedral arrangement together with the stereochemically active $6s^2$ lone electron pair of Bi^{3+}. The unique structure of $Bi_{12}TiO_{20}$ exhibits a number of interesting properties, including piezoelectric, electro-optical, and photoconductive properties [8].

Many studies show that $Bi_{12}TiO_{20}$ have attracted a lot of attention due to their easy processability via a variety of methods,

*Corresponding author. Tel.: +55 16 98237 2970.
E-mail address: andreesteves86@hotmail.com (A.E. Nogueira).

http://dx.doi.org/10.1016/j.ceramint.2015.06.024
0272-8842/© 2015 Elsevier Ltd and Techna Group S.r.l. All rights reserved.

high photocatalytic activity, non-toxicity, small band gap, etc. [9,10]. The literature reports different synthesis methods for obtaining bismuth titanate such as the precipitation method [11], chemical solution decomposition process method [12], hydrothermal method [13], combustion synthesis technique [10], etc. However, these methods still have limitations such as high calcining temperature, complicated manipulation, and high consumption of organic agents which may affect the photocatalytic properties of semiconductors.

In this context, the oxidant peroxide method (OPM) has been used to produce highly reactive ceramic powders with a variety of particle morphologies, sizes and compositions [14,15]. The main innovation of this route is the possibility of obtaining nanosized ceramic powders of great technological and commercial interest, free of any contamination by carbon and halides [16,17]. Other important characteristics of this new technique, which represents a huge environmental gain, is the exclusive use of water as a solvent, low temperature processing used for crystallization of nanosized oxides and the absence of any potentially toxic byproduct.

In the present work, we prepared $Bi_{12}TiO_{20}$ photocatalysts, calcined at different temperatures, by the oxidant peroxide method (OPM), and the investigated the effects of calcination temperature on the structural properties of $Bi_{12}TiO_{20}$, such as morphology, crystal structure and optical properties, in detail. Furthermore, the effects of calcination temperature on the photocatalytic activity of $Bi_{12}TiO_{20}$ were investigated by the photocatalytic degradation of RhB solution.

2. Materials and methods

2.1. Preparation of materials

An amorphous precipitate with molar ratio (Bi:Ti=12:1) was synthesized as described by Camargo and Kakihana [16] through the addition of 0.0250 g of titanium metal powder (98% Aldrich, USA) in an aqueous solution of 60 mL of H_2O_2 (30%, analytical grade, Synth, Brazil) and 40 mL of ammonia aqueous solution (30%, analytical grade, Synth, Brazil). After approx. 3 h, a yellow transparent solution of peroxytitanate complexes was obtained, and a second solution of 3.28 g of Bi_2O_3 (99.99%, Aldrich, USA) added into 30 mL of diluted nitric acid (analytical grade, Synth, Brazil) was slowly added dropwise to the peroxytitanate solution under stirring and cooling in an ice-water bath. The result was a vigorous evolution of gas, forming a yellow precipitate that was filtered and washed with diluted ammonia solution to eliminate all of the nitrate ions. The washed precipitate was dried at 60 °C for 3 h, ground and calcined at several temperatures between 400 and 700 °C for 1 h at a heating rate of 10 °C min^{-1} in closed alumina boats.

2.2. Characterization of the materials

The precursor and all of the calcined powders were characterized by infrared absorption spectroscopy with a Fourier transform infrared (FTIR) spectrometer (Bruker EQUIXOX 55, Ettlingen, Germany) with an attenuated total reflectance accessory (ZnSe monocrystal). The spectra were collected at room temperature in the 400–4000 cm^{-1} range, with 32 scans and 4 cm^{-1} resolution. All the powders (precipitate and heat-treated) were characterized at room temperature by XRD using the CuKα radiation (Rigaku D/MAX 200, with a rotary anode operating at 150 kV and 40 mA) in the 2θ range from 10° to 75° with step scan of 0.02°. The specific surface areas of the sample were determined through nitrogen adsorption at 77 K (Micromeritics ASAP 2000). Diffuse reflectance spectroscopy in ultraviolet visible (DRS) range spectra were recorded by using a Varian model Cary 5G in the diffuse reflectance mode and transformed to a magnitude proportional to the extinction coefficient through the Kubelka–Munk function, scans range was 200–800 nm.

Thermogravimetric analysis was evaluated using a TGA Q500 thermogravimetric analyzer (TA Instruments, New Castle, DE) under the following conditions: weight 10.00 ± 0.50 mg; synthetic air flow 60 mL/min; heating rate 100 °C/min; and temperature range of 25–600 °C. A small amount of the dry precipitate (10.0 mg) was characterized by differential scanning calorimetry (DSC 404 C controlled by TASC 424/3A, Netzsch, Germany) between 25 and 550 °C using an aluminum crucible and a constant heating/cooling rate of 10 °C/min with a flux of 0.50 cm^3/min. The morphology of the powders was characterized by transmission electron microscope (TEM) FEI/PHILIPS CM120 and field emission scanning electron microscopy (FESEM, ZEISS model-SUPRA 35). Photoluminescence (PL) properties were measured with a Thermal Jarrel-Ash Monospec 27 monochromator and a Hamamatsu R446 photomultiplier. The excitation source was a 350.7 nm wavelength of a krypton ion laser (Coherent Innova), keeping its power at 15 mW.

2.3. Catalytic tests

The RhB dye is used as a model compound in oxidation reactions for presenting strong absorption in the visible area (λ_{max}=554 nm), high solubility in water and properties similar to those presented by the textile dyes, which are difficult to degrade.

Eighty milliliters of a 10 mg L^{-1} solution of RhB dye at pH 6.0 were mixed with 60 mg of the catalyst and irradiated with visible light inside a box. The light sources were set at a distance of 20 cm from the beaker containing the catalyst and RhB dye. The visible radiation was obtained with six lamps (PHILIPS TL-D, 15W with maximum intensity at 440 nm). All photocatalytic tests were performed in quadruplicate. For the adsorption test, we used the same conditions except for the presence of radiation. Reactions were monitored by UV–vis spectroscopy (JASCO V-660) at 554 nm, using a commercial quartz cuvette.

3. Results and discussion

3.1. Characterization of the materials

The solid state reaction is the most common and oldest method for obtaining ceramic powder. This method consists of mixing the reactants such as oxides, carbonates or hydroxides in a mill to homogenize and reduce the particle size, followed

by heat treatment to allow interdiffusion of cations to form the crystalline material.

Conventionally, bismuth titanate is prepared by solid state reaction using bismuth oxide (Bi_2O_3) and titanium oxide (TiO_2) as starting materials. However, this method requires long grinding times for homogenization and high calcination temperatures, resulting in materials with some undesirable characteristics such as a wide particle size distribution and loss of stoichiometry due to volatilization of the reagents at high temperatures [18].

Thus, in order to obtain single-phase materials with improved chemical and physical properties, the OPM method was used for obtaining the bismuth titanate with sillenite phase ($Bi_{12}TiO_{20}$). In this method, peroxytitanate complexes synthesized in situ act similarly to H_2O_2 molecules according to the following equations (1) and (2) [16].

$$Pb(OH)^{2-}_{4(aq)} + 2H_2O_{2(aq)} \rightarrow PbO_{2(s)} + 2H_2O_{(l)} + 2OH^-_{(aq)} \quad (1)$$

$$Pb(OH)^{2-}_{4(aq)} + \left[Ti(OH)_3O_2\right]^-_{(aq)} \rightarrow PbO_{2(s)} + TiO_{2(s)} + 2H_2O_{(l)} + 3OH^-_{(aq)} \quad (2)$$

The peroxytitanate complexes are obtained from the titanium metal with a hydrogen peroxide and ammonia solution, forming the peroxotitanate ion $[Ti(OH)_3O_2]^-$, which has a characteristic yellow color of peroxo complexes [16].

HOU et al. proposed a peroxotitanate ion formation mechanism, wherein the oxygen radical formed during the Ti/H_2O_2 interaction binds to titanium [19]. The superoxide formed is subsequently replaced by hydroxyl in the sphere of internal titanium coordination due to the high pH (Eq. (3)).

$$Ti_{(s)} + 3HO^-_{2(aq)} + H_2O_{(l)} \rightarrow \left[Ti(OH)_3O_2\right]^-_{(aq)} + HO^-_{(aq)} \quad (3)$$

The reaction between peroxytitanate complexes with bismuth ions in solution results in the formation of a yellow precipitate, which is defined as a mixture of bismuth and amorphous titanium oxide [19].

When the bismuth nitrate solution comes into contact with the solution of the peroxytitanate complexes, there is a rise in pH and formation of $Bi(OH)_5$, which is reduced exothermically in the presence of H_2O_2, forming the amorphous bismuth oxide (Bi_2O_3) according to Eq. (3). Simultaneously, there is the hydrolysis of peroxytitanate complexes forming the $Ti(OH)_4$, due to the formation of H_2O by oxidation of hydrogen peroxide according to Eq. (4), forming the amorphous precursor, which after heat treatment, results in crystalline bismuth titanate.

$$Bi(OH)_{5(s)} + H_2O_{(aq)2} \rightarrow Bi_2O_{3(s)} + H_2O_{(l)} + OH^-_{(aq)} \quad (4)$$

$$\left[Ti(OH)_3O_2\right]^-_{(aq)} + H_2O_{(l)} \rightarrow Ti(OH)_{4(s)} + O_{4(g)} + OH^-_{(aq)} \quad (5)$$

The thermal stability of the precipitate obtained by the OPM method was evaluated by thermogravimetric analysis (Fig. 1).

Fig. 1 shows that the precipitate weight loss of about 9 wt% in two stages, the first step is from 25 to 400 °C, with 5 wt% weight loss, which is associated with the evaporation of absorbed water. The second stage, between 400 and 530 °C, related to the $BiONO_3$ was decomposed to Bi_2O_3. For temperatures above 530 °C, the weight loss is negligible and the weight of the precipitate appears to be constant. The exothermic peak at approximate 376 °C is

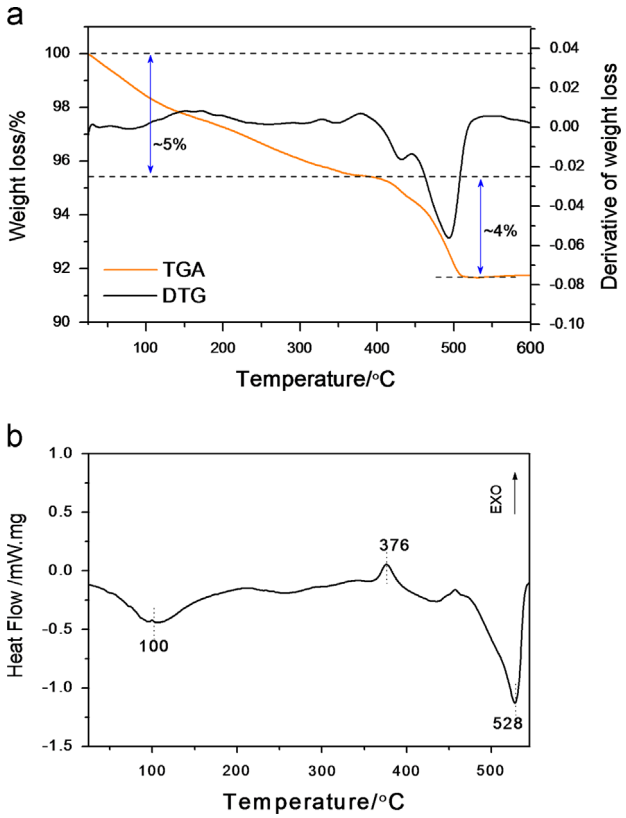

Fig. 1. Thermogravimetric analysis (a) and differential scanning calorimetry (b) patterns of precipitate; the heating rate was 10 °C/min.

ascribed to the crystallization of precipitate from the amorphous phase [19].

The phase and structure of the as-synthesized samples were examined by XRD (Fig. 2). The XRD of materials calcined above 500 °C exhibits a single phase related to $B_{12}TiO_{20}$ with space group I23 (PDF-0097). However, the material calcined at 400 °C showed a secondary phase marked with the symbol ♦ related to the prerovskita phase of bismuth titanate ($Bi_4Ti_3O_{12}$) (PDF35-0795). This phase is metastable during the sillenite phase forming process and disappears with increasing calcination temperature, as reported by Zhang et al. in the preparation of $Bi_{12}TiO_{20}$ films by chemical solution deposition [8].

The average crystal size of bismuth titanate was estimated to the full width at half-maximum (FWHM) of the (3 1 0) peak of sillenite by applying the Scherrer equation as follows [20]:

$$D = \frac{K\lambda}{\beta \cos \theta} \quad (6)$$

where K is a constant (shape factor, about 0.94), λ is the X-ray wavelength ($\lambda = 0.15406$), β is the FWHM of the diffraction line, and θ is the diffraction angle. The results are presented in Table 1. We can see from the table that, with the increase in calcination temperature, the crystal size of $Bi_{12}TiO_{20}$ increases gradually.

The infrared spectrum of the precipitate showed a broad band between 400 and 800 cm^{-1} (Fig. 3a), while in the calcined material this band is divided into four bands at 467, 527, 594 and 673 cm^{-1}, corresponding to the vibration modes

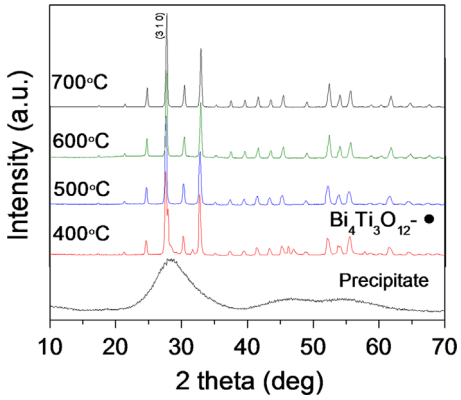

Fig. 2. X-ray diffraction patterns of the powder precipitated and calcined at different temperatures for 1 h.

Table 1
Crystal size and specific surface area of the materials.

Sample (°C)	Crystal size (nm)	S_{BET} ($m^2\ g^{-1}$)
400	57	6.62
500	59	5.45
600	67	4.46
700	83	2.49

of the Bi–O and Ti–O characteristic of bismuth titanate with selenite phase as observed by Carvalho et al. [21]. It was also observed that with increasing calcination temperature, the spectra showed sharper bands, indicating an alignment of the cubic structure of sillenite, corroborating the XRD results (Fig. 2) [13,22]. The band centered at 3490 cm^{-1} is attributed to the stretching vibration of the O–H bond, which may be due to the presence of surface adsorbed water molecules and the band centered at 1400 cm^{-1} is attributed to the antisymmetric stretching vibration of these peaks decreasing, with increasing calcination temperatures.

The detailed morphological characterization of materials were examined by FESEM and TEM (Fig. 4). The FESEM images of calcined samples show the presence of large particles of complex shape formed from the partial sintering of smaller primary particles. The outstanding features of the OPM powders are their reactivity, which could be confirmed in the FESEM images by the presence of partially sintered particles and by the formation of necks between them. TEM images of the precipitate show irregular clusters of particles, along with well-defined spherical particles of different sizes which may be related to bismuth oxide as shown in previous studies [23].

In terms of textural analysis, the specific surface area was calculated by the BET equation. The precipitate shows a specific surface area of 21.6 $m^2\ g^{-1}$; however, there was a decrease in the surface area of the materials with the increase of calcination temperature, showing a surface area of 6.62 and 2.49 $m^2\ g^{-1}$ for the materials calcined at 400 and 700 °C, respectively, due to the process of crystallization and sintering of particles.

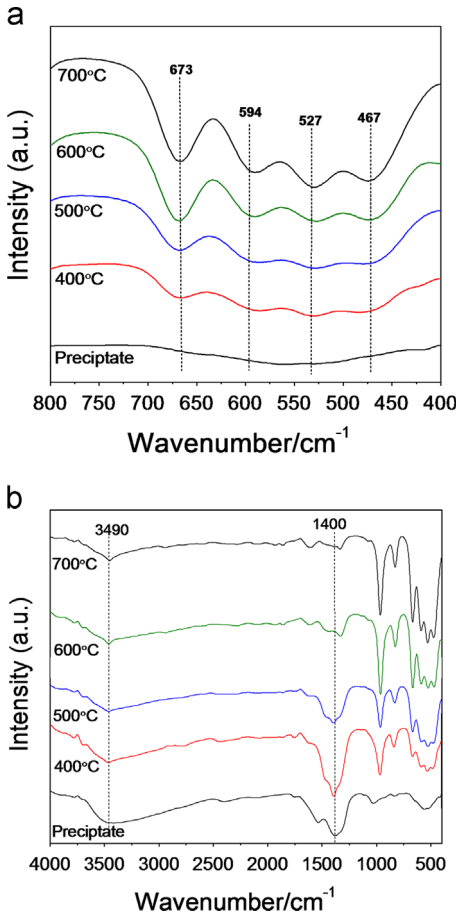

Fig. 3. FTIR spectra in the 400–800 cm^{-1} region (a) and the 400–4000 cm^{-1} region (b) of the powder precipitated and calcined at different temperatures for 1 h.

The specific surface area of a catalyst affects the heterogeneous catalysis processes, since an increase in specific surface area causes an increase in the number of active sites on the catalyst surface, which is directly related to an increase in the reaction rate of the process. However, studies have shown that the catalytic activity of bismuth titanate should not only the specific surface area, but also the structural defects generated, which depend on the synthesis method as well as of the heat treatment used [24].

UV–vis diffuse reflectance is used to characterize the optical properties of as-synthesized samples (Fig. 5). The band gaps of the samples were further determined by fitting the optical transition at the absorption edges using the Tauct model described by the equation $(\alpha h\nu)^n = A(h\nu - E_g)$, where h is Planck's constant, ν the frequency of vibration, α the absorption coefficient, E_g the band gap, and A is the proportional constant. The value of the exponent n is dependent on the type of transition between the semiconductor bands, where $n=2$ for direct transition and $n=1/2$ for indirect transition [25,26].

In the DRS spectra of the materials it was observed that increasing calcination temperature caused a shift of the absorption edge to longer wavelengths, which means a band gap energy decrease in the materials, as can be seen in Fig. 5b.

The results show the band gap energy of the oscillation with increasing calcination temperature, which may be related to the

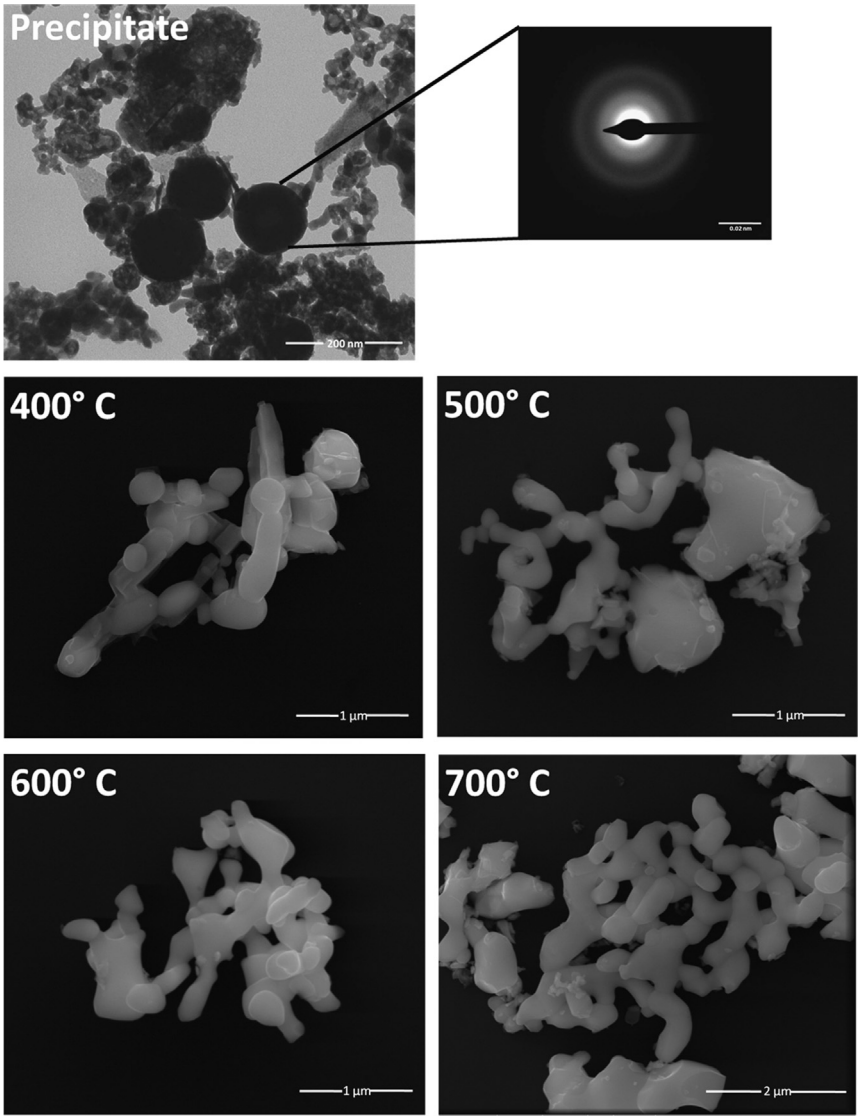

Fig. 4. TEM image of the precipitate powder and FESEM images of the calcined materials at different temperatures for 1 h.

different densities of structural and superficial defects present in each sample. As the defects cannot be controlled in the materials, their presence only provides a change in the amount and distribution of intermediate energy levels within the band gap region.

The band gap energy estimated for the materials showed a value under 2.66 eV, with an absorption onset from 466 nm. This indicates that bismuth titanates prepared by the OPM method are sensitive to visible irradiation, representing a possible photoactivity under solar irradiation.

Photoluminescence (PL) spectroscopy was used as a complementary tool for DRS measurements to assist in understanding the organization of the electronic structure. PL spectra of the materials synthesized by the OPM method calcination at different temperatures are shown in Fig. 6.

PL spectra of these materials show broad bands with maximum emission in the green and red region of the visible electromagnetic spectrum. Variations can be seen in the luminescence response as the calcining temperature of the materials increased high, which can be assigned to different types of defects and defect densities, characteristic to each material. The material calcined at 400, 500 and 600 °C has a maximum emission at 632 nm and the material calcined at 700 °C shows a maximum at 550 nm. The PL emission from the materials can be related to the presence of energy levels located in the band gap, known as deep donors, that are responsible for PL emissions in the regions of green, yellow, orange and red of the electromagnetic spectrum [27].

3.2. Catalytic tests

The first test performed was the direct photolysis of RhB. This process is related to the degradation of organic compounds accomplished solely by the presence of electromagnetic radiation. In this way, in order to evaluate the influence of photolysis during the photocatalysis process, measurements were performed under visible radiation in the absence of the semiconductor. It was observed that after 240 min of reaction, there was 6% discoloration the RhB dye solution (Fig. 7a). It is important to emphasize

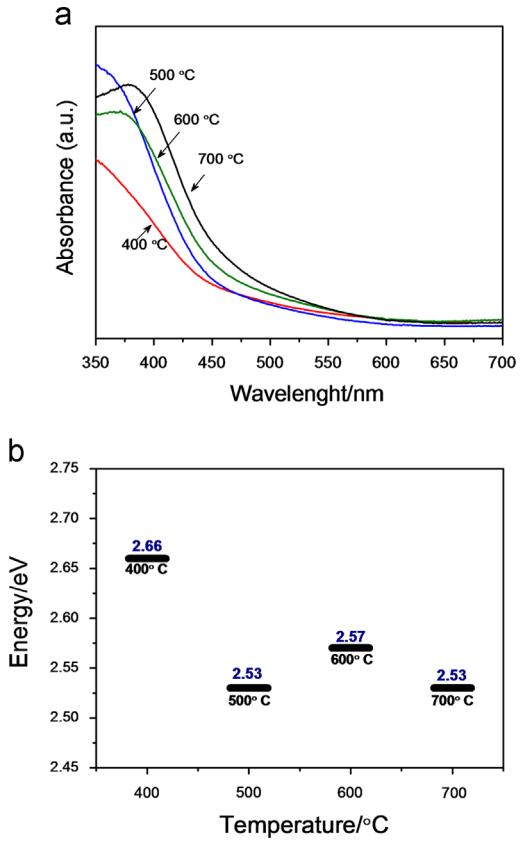

Fig. 5. (a) UV–vis diffuse reflectance spectra and (b) band gap energies of samples calcined at different temperatures for 1 h.

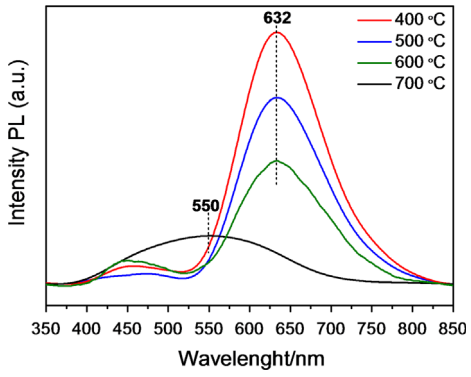

Fig. 6. Photoemission spectra of materials calcined at different temperatures for 1 h. The excitation was carried out using a krypton ion laser at 350.7 nm wavelength.

that the results of photocatalysis presented below include the effects of photolysis.

The kinetic adsorption process obtained a maximum of about 7% RhB dye discoloration after 210 min. It is observed that the concentration of the RhB dye varies up to 60 min of reaction, while remaining constant after that time, which indicates that the adsorption–desorption equilibrium was reached.

The photocatalytic activity of the materials was evaluated by the degradation of RhB aqueous solution under visible light irradiation. Fig. 8 shows the RhB dye discoloration efficiency of calcined materials at 400 and 500 °C were the highest among all samples under visible light irradiation, about 71% and 68% of the RhB dye solution was discolored within 210 min respectively.

To get a high photocatalytic activity, the photoexcited electron/hole pairs should effectively be migrated to the catalyst surface of catalyst and take part in the oxidation/reduction reaction before their recombination. Thus, the migrated distance greatly affects the utilization efficiency of photoexcited electron/hole pairs. Smaller crystal size means shorter distance that photoexcited electron/hole pairs should migrate, which reduces the recombination probability of electron/hole pairs and improves the photocatalytic activity of semiconductors. From Table 1, we can see that with the increase in calcination temperature, the crystal size of $Bi_{12}TiO_{20}$ also increases, which is detrimental to photocatalytic activity of $Bi_{12}TiO_{20}$.

The kinetic rate constants of the samples were obtained by plotting ln C/C_0 with the visible light irradiation time, which is shown in Fig. 8b. The photocatalytic degradation of RhB over the photocatalysts matches the pseudo-first-order kinetics equation ($-dc/dt = kc$). The kinetic rate constant over 400 °C is 0.006 min^{-1}, which is 9.4 times higher than commercial TiO_2 with anatase phase (99.70%, Aldrich, USA) (Table 2). This is because $Bi_{12}TiO_{20}$ has a middle gap that accelerates the production of photo-generated electrons and holes under

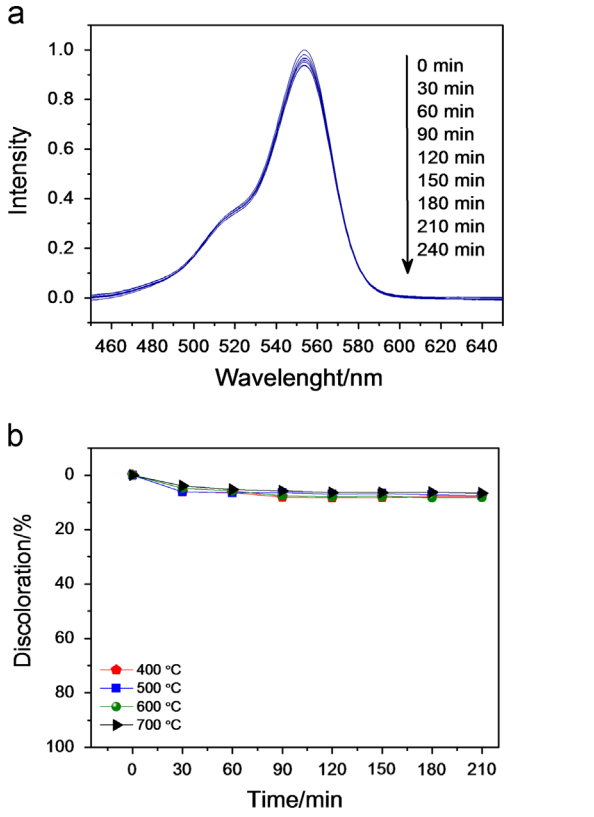

Fig. 7. Absorbance spectra changes of RhB solution (10 mg/L) after different irradiation times without catalyst under visible radiation (a) and kinetic adsorption curves of RhB dye with materials calcined at different temperatures for 1 h.

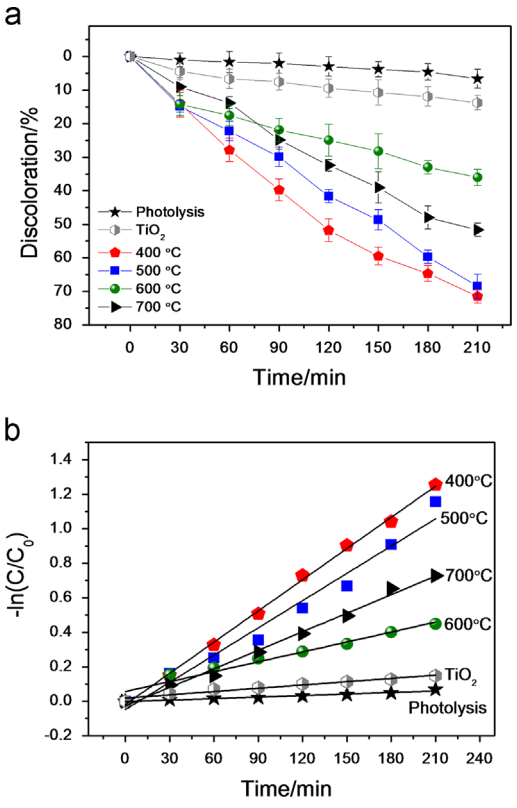

Fig. 8. Kinetics of photocatalytic decomposition of RhB (a) and the first-order kinetics equation (b) patterns of commercial TiO_2 and bismuth titanate calcined at different temperatures for 1 h under visible radiation.

Table 2
The photocatalytic degradation efficiency and reaction rate constants of materials calcined at different temperatures for 1 h.

Sample	RhB degradation (%)	$k \times 10^{-3}$ (min^{-1})	Error (10^{-4})	R^2
Photolysis	7	0.29	± 0.25	0.9533
TiO_2	14	0.64	± 0.53	0.9535
400 °C	71	6.02	± 1.08	0.9977
500 °C	68	5.26	± 3.47	0.9703
600 °C	36	1.91	± 1.60	0.9529
700 °C	51	3.58	± 1.37	0.9898

visible light, and as a result it is easier to degrade RhB into CO_2 and H_2O. The commercial TiO_2 has the band gap of 3.2 eV and cannot utilize visible light, so it has weak photocatalytic activity under visible light.

4. Conclusion

This work demonstrated that single phase of $Bi_{12}TiO_{20}$ powders may be produced by the OPM method by employing a calcination temperature of 500 °C for 1 h with heating/cooling rates of 10 °C/min and the DRS confirmed that the photoresponse of the prepared bismuth titanate extended to the visible light region at about 465 nm representing a possible photoactivity under solar irradiation. The as-prepared materials exhibited excellent photocatalytic performance toward degradation of RhB under visible radiation. The material calcined at 400 °C shows the highest photocatalytic activity, which is about 9.4 times higher than commercial TiO_2.

References

[1] H. Sun, G. Zhou, S. Liu, H.M. Ang, M.O. Tadé, S. Wang, Visible light responsive titania photocatalysts codoped by nitrogen and metal (Fe, Ni, Ag, or Pt) for remediation of aqueous pollutants, Chem. Eng. J. 231 (2013) 18–25.
[2] M. Pelaez, N.T. Nolan, S.C. Pillai, M.K. Seery, P. Falaras, A.G. Kontos, P.S.M. Dunlop, J.W.J. Hamilton, J.A. Byrne, K. O'Shea, M.H. Entezari, D.D. Dionysiou, A review on the visible light active titanium dioxide photocatalysts for environmental applications, Appl. Catal. B 125 (2012) 331–349.
[3] D. Spasiano, R. Marotta, S. Malato, P. Fernandez-Ibañez, I. Di Somma, Solar photocatalysis: materials, reactors, some commercial, and pre-industrialized applications. A comprehensive approach, Appl. Catal. B 170–171 (2015) 90–123.
[4] T. Lin, Z. Pi, M.C. Gong, J.B. Zhong, J.L. Wang, Y.Q. Chen, Gas-phase photocatalytic oxidation of benzene over titanium dioxide loaded on $Bi_{12}TiO_{20}$, Chin. Chem. Lett. 18 (2007) 241–243.
[5] S.R. Thakare, G.S. Gaikwad, N.T. Khati, A.V. Wankhade, Development of new, highly efficient and stable visible light active photocatalyst Ag_2ZrO_3 for methylene blue degradation, Catal. Commun. 62 (2015) 39–43.
[6] J. Zhang, Y. Hu, X. Jiang, S. Chen, S. Meng, X. Fu, Design of a direct Z-scheme photocatalyst: preparation and characterization of Bi_2O_3/g-C_3N_4 with high visible light activity, J. Hazard. Mater. 280 (2014) 713–722.
[7] W.T. Li, W.Z. Huang, H. Zhou, H.Y. Yin, Y.F. Zheng, X.C. Song, Synthesis and photoactivity enhancement of Ba doped Bi_2WO_6 photocatalyst, Mater. Res. Bull. 64 (2015) 432–437.
[8] H. Zhang, M. Lü, S. Liu, Z. Xiu, G. Zhou, Y. Zhou, Z. Qiu, A. Zhang, Q. Ma, Preparation and photocatalytic properties of sillenite $Bi_{12}TiO_{20}$ films, Surf. Coat. Technol. 202 (2008) 4930–4934.
[9] X. Zhu, J. Zhang, F. Chen, Hydrothermal synthesis of nanostructures $Bi_{12}TiO_{20}$ and their photocatalytic activity on acid orange 7 under visible light, Chemosphere 78 (2010) 1350–1355.
[10] O. Subohi, G.S. Kumar, M.M. Malik, Optical properties and preparation of bismuth titanate ($Bi_{12}TiO_{20}$) using combustion synthesis technique, Optik 124 (2013) 2963–2965.
[11] N. Thanabodeekij, E. Gulari, S. Wongkasemjit, $Bi_{12}TiO_{20}$ synthesized directly from bismuth (III) nitrate pentahydrate and titanium glycolate and its activity, Powder Technol. 160 (2005) 203–208.
[12] W. Feng Yao, H. Wang, X. Hong, Xu, X. Feng Cheng, J. Huang, S. Xia Shang, X. Na Yang, M. Wang, Photocatalytic property of bismuth titanate $Bi_{12}TiO_{20}$ crystals, Appl. Catal. A 243 (2003) 185–190.
[13] X. Zhu, J. Zhang, F. Chen, Study on visible light photocatalytic activity and mechanism of spherical $Bi_{12}TiO_{20}$ nanoparticles prepared by low-power hydrothermal method, Appl. Catal. B 102 (2011) 316–322.
[14] A.E. Nogueira, E. Longo, E.R. Leite, E.R. Camargo, Synthesis and photocatalytic properties of bismuth titanate with different structures via oxidant peroxo method (OPM), J. Colloid Interface Sci. 415 (2014) 89–94.
[15] E.R. Camargo, M.G. Dancini, M. Kakihana, The oxidant peroxo method (OPM) as a new alternative for the synthesis of lead-based and bismuth-based oxides, J. Mater. Res. 29 (2014) 131–138.
[16] E.R. Camargo, M. Kakihana, Peroxide-based route free from halides for the synthesis of lead titanate powder, Chem. Mater. 13 (2001) 1181–1184.
[17] E.R. Camargo, J. Frantti, M. Kakihana, Low-temperature chemical synthesis of lead zirconate titanate (PZT) powders free from halides and organics, J. Mater. Chem. 11 (2001) 1875–1879.
[18] M. Kakihana, Invited review "sol–gel" preparation of high temperature superconducting oxides, J. Sol-Gel Sci. Technol. 6 (1996) 7–55.

[19] J. Hou, Y. Qu, D. Krsmanovic, R.V. Kumar, Peroxide-based route assisted with inverse microemulsion process to well-dispersed $Bi_4Ti_3O_{12}$ nanocrystals, J. Nanopart. Res. 12 (2009) 1797–1805.

[20] J.I. Langford, A.J.C. Wilson, Scherrer after sixty years: a survey and some new results in the determination of crystallite size, J. Appl. Crystallogr. 11 (1978) 102–113.

[21] J.F. Carvalho, R.W.A. Franco, C.J. Magon, L.A.O. Nunes, A.C. Hernandes, Optical and magnetic characterization of pure and vanadium-doped $Bi_{12}TiO_{20}$ sillenite crystals, Opt. Mater. 13 (1999) 333–338.

[22] S. Kojima, R. Imaizumi, S. Hamazaki, M. Takashige, Raman scattering study of bismuth layer-structure ferroelectrics, Jpn. J. Appl. Phys. 33 (1994) 5559.

[23] A. Nogueira, A.F. Lima, E. Longo, E. Leite, E. Camargo, Structure and photocatalytic properties of Nb-doped $Bi_{12}TiO_{20}$ prepared by the oxidant peroxide method (OPM), J. Nanopart. Res. 16 (2014) 1–10.

[24] O. Merka, D.W. Bahnemann, M. Wark, Photocatalytic hydrogen production with non-stoichiometric pyrochlore bismuth titanate, Catal. Today 225 (2014) 102–110.

[25] D.L. Wood, J. Tauc, Weak absorption tails in amorphous semiconductors, Phys. Rev. B Condens. Mater. 5 (1972) 3144–3151.

[26] L. Tolvaj, K. Mitsui, D. Varga, Validity limits of Kubelka–Munk theory for DRIFT spectra of photodegraded solid wood, Wood Sci. Technol. 45 (2011) 135–146.

[27] S.K. Rout, L.S. Cavalcante, J.C. Sczancoski, T. Badapanda, S. Panigrahi, M. Siu Li, E. Longo, Photoluminescence property of powders prepared by solid state reaction and polymeric precursor method, Phys. B Condens. Matter 404 (2009) 3341–3347.